

# Preparation and Characterization of Dinuclear Nickel(II) Complexes Containing $N_3Ni(\mu_{1,3}\text{-SO}_3R)_2(\mu\text{-RCN}_4)NiN_3$ Cores: Crystal Structures and Magnetic Properties

Jochen Lach,<sup>[a]</sup> Eva Perlt,<sup>[b]</sup> Barbara Kirchner,<sup>[b]</sup> and Berthold Kersting\*<sup>[a]</sup>

**Keywords:** Macrocyclic ligand; Sulfonato donors; Nickel; Magnetic properties; Crystal structure; Tetrazolates; DFT calculations

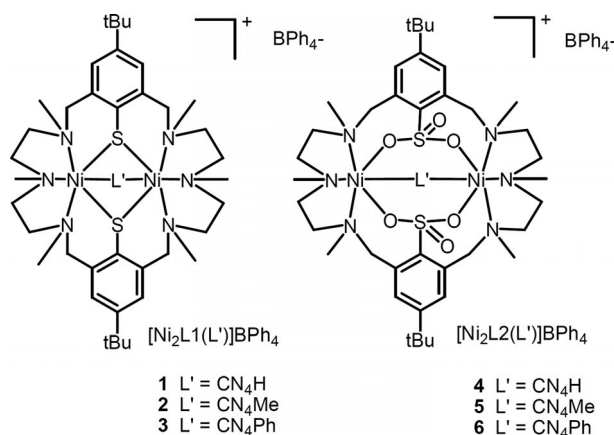
**Abstract.** The preparation and characterization of three new mixed ligand macrocyclic  $[Ni_2L_2(L')^+]^+$  complexes are described, where  $(L_2)^{2-}$  represents a supporting macrocyclic hexaaza-bis(phenylsulfonato) ligand and  $L'$  a tetrazolato ligand. The complexes  $[Ni_2(L_2)(CN_4H)]BPh_4$  (**4**),  $[Ni_2(L_2)(CN_4Me)]BPh_4$  (**5**), and  $[Ni_2(L_2)(CN_4Ph)]BPh_4$  (**6**) were synthesized by  $H_2O_2$  oxidation of the corresponding  $[Ni_2(L_1)(CN_4H)]BPh_4$  (**1**),  $[Ni_2(L_1)(CN_4Me)]BPh_4$  (**2**), and  $[Ni_2(L_1)(CN_4Ph)]BPh_4$  (**3**) complexes supported by the corresponding hexaaza-bis(thiophenolate) macrocycle. The compounds were characterized by means of elemental analysis, mass spectrometry, IR, and UV/Vis spectroscopy. The crystal structures of compounds **4–6** show that the bridging thiophenolate functions in **1–3** are in all

cases converted to  $\mu_{1,3}$ -bridging sulfonato groups to generate  $N_3Ni(\mu_{1,3}\text{-SO}_3R)_2(\mu\text{-RCN}_4)NiN_3$  cores. The conversion to the phenylsulfonato groups is accompanied by a drastic increase of the Ni...Ni distances from 3.455(1) Å in **1**, 3.425(1) Å in **2**, and 3.443(1) Å [3.450(1) Å] in **3** to 4.2796(5) Å [4.3375(6) Å] in **4**, 4.3402(6) Å in **5**, and 4.2607(4) Å in **6**. Upon oxidation the magnetic properties are affected. In contrast to **1–3**, which exhibit an intramolecular ferromagnetic exchange interaction ( $S = 2$  ground state), the spins of the nickel(II) ( $S_i = 1$ ) ions in **4–6** are antiferromagnetically coupled, the coupling constants  $J$  being  $-1.39\text{ cm}^{-1}$  (**4**),  $-1.43\text{ cm}^{-1}$  (**5**), and  $-1.60\text{ cm}^{-1}$  (**6**) ( $H = -2JS_1S_2$ ) to yield a diamagnetic  $S = 0$  ground state. DFT (density functional theory) calculations were carried out to substantiate the experimental results.

## Introduction

In the past several years we have characterized a number of dinuclear transition metal complexes supported by the macrocyclic hexaaza-bis(thiophenolate) ligand  $H_2L_1$ .<sup>[1]</sup> With first row transition metal ions such as  $Ni^{2+}$ ,  $Co^{2+}$ ,  $Fe^{2+}$ , and  $Mn^{2+}$  the doubly deprotonated macrocycle  $(L_1)^{2-}$  invariably forms mixed-ligand  $[M_2(L_1)(L')^+]^+$  complexes with a bioctahedral  $N_3M(\mu\text{-SR})_2(\mu\text{-L}')MN_3$  core structure, where  $L'$  represents a bridging coligand (Scheme 1).<sup>[2–5]</sup> The complexes are distinguished by the bowl-shaped binding cavity that confers some unusual properties on the complexes.<sup>[6]</sup> We have also investigated the coordination chemistry of the hexaaza-disulfonato ligand  $H_2L_2$ , but to a lesser extent. Analogous pairs of dinuclear  $[Ni_2(L_1)(L')^+]^+$  and  $[Ni_2(L_2)(L')^+]^+$  complexes have been reported with  $L' = Cl^-$ ,  $CH_3CO_2^-$ ,  $PhCO_2^-$ ,  $3\text{-Cl-C}_6\text{H}_4\text{CO}_2^-$ .<sup>[7,8]</sup> It was found that the structures and chemical properties are strikingly different, a fact attributable to the conversion of the

bridging thiophenolate to phenylsulfonato groups. On these grounds we decided to prepare and characterize further examples of analogous complexes of the dinucleating macrocycles  $(L_1)^{2-}$  and  $(L_2)^{2-}$ . In this study, we have selected the tetrazolates  $RCN_4^-$  ( $R = H, Me, Ph$ ) as coligands.



**Scheme 1.** Structures of  $[Ni_2(L_1)(CN_4R)]BPh_4$  (**1–3**) and  $[Ni_2(L_2)(CN_4R)]^+$  (**4–6**).

Herein, we report on the preparation, structures, and magnetic properties of the three tetrazolato-bridged  $[Ni_2(L_2)(CN_4R)]^+$  complexes **4–6** ( $R = H, Me, Ph$ ) (Scheme 1). Their structures and magnetic properties are discussed and compared with those of their reduced

\* Prof. Dr. B. Kersting  
E-Mail: b.kersting@uni-leipzig.de  
[a] Institut für Anorganische Chemie  
Universität Leipzig  
Johannisallee 29  
04103 Leipzig, Germany

[b] Wilhelm-Ostwald-Institut für Physikalische und Theoretische Chemie  
Linnéstraße 2  
04103 Leipzig, Germany

Supporting information for this article is available on the WWW under <http://dx.doi.org/10.1002/zaac.201200501> or from the author.

$[Ni_2(L1)(CN_4R)]^+$  parents (**1–3**), which have been reported earlier.<sup>[3,4]</sup>

## Results and Discussion

### Syntheses of Metal Complexes

The route to the new compounds **4–6** used the complexes **1–3** as starting materials. These complexes were synthesized according to published procedures, and subjected to direct oxidations using excess of  $H_2O_2$  as an oxidant.<sup>[4]</sup> This oxidant converts thiophenolate complexes to sulfonate complexes.<sup>[9–11]</sup> In previous work, we always used the perchlorate salts in such oxidation reactions.<sup>[7]</sup> We now found that this method works for the tetraphenylborate salts as well. Thus, the reaction of green  $[Ni_2(L1)(CN_4H)][BPh_4]$  (**1**) with an excess of  $H_2O_2$  in methanol solution provided the pale-green salt  $[Ni_2(L2)(CN_4H)][BPh_4]$  (**4**) in 67% yield. The tetraphenylborate salts **2** and **3** reacted in the same fashion yielding pale-green **5** and **6** in reproducible yields as high as 63% and 64%, respectively. All compounds are stable in air in the solid state and in solution.

### Spectroscopic Characterization of Metal Complexes

The composition of the compounds was confirmed by means of elemental analysis, mass spectrometry, IR, and UV/Vis spectroscopy. Selected analytical data are listed in Table 1. The electrospray ionization mass spectra (ESI-MS) of dilute MeCN solutions of **4–6** exhibit molecular ion peaks at  $m/z = 949.20$ ,  $m/z = 963.34$ , and  $m/z = 1025.36$  with the correct isotopic distribution for the  $[Ni_2(L2)(CN_4R)]^+$  cations. Selected IR and UV/Vis data for **4–6** are shown in Table 1. In the IR spectra of **4–6** the most prominent features are the strong absorption bands at ca.  $1200\text{ cm}^{-1}$ , which are attributable to the S–O

stretching vibration of sulfonate ( $RSO_3^-$ ) groups.<sup>[8,10,12,13]</sup> The S–O frequencies resemble those of the  $Ni_2$  complexes  $[Ni_2(L2)(L')]$  ( $L' = Cl^-, O_2CMe^-, O_2CPh^-, O_2C-C_6H_4-3Cl^-$ ) that were investigated earlier, indicating that the  $RSO_3^-$  groups in **4–6** are also in a  $\mu_{1,3}$ -bridging mode.<sup>[7,8]</sup>

UV/Vis spectroscopic data of **4–6** were recorded from 190–1600 nm in acetonitrile solution at room temperature with a Jasco V-670 UV/Vis/NIR spectrophotometer. The most obvious spectral differences among the thiophenolate and phenylsulfonate complexes occur in the UV/Vis region around 400 nm. The thiophenolato complexes display strong thiolate  $\rightarrow Ni^{2+}$  charge transfer transitions in this region.<sup>[4]</sup> The phenylsulfonato complexes in **4–6** lack this transition, in agreement with the conversion of the soft thiolate to hard sulfonate groups. As a consequence, the spin-allowed  $^3A_{2g}(F) \rightarrow ^3T_{1g}(P)$  transition, which is expected for a  $Ni^{2+}$  ion with octahedral coordination, but which is obscured in **1–3** by strong  $RS^- \rightarrow Ni^{2+}$  charge transfer transitions, can be detected as a weak absorption band at 441–443 nm. The remaining bands in the 630 nm and 1030 nm regions can be attributed to the spin-allowed d–d transitions  $^3A_{2g}(F) \rightarrow ^3T_{1g}(F)$  [ $v_2$ ] and  $^3A_{2g}(F) \rightarrow T_{2g}(F)$  [ $v_1$ ] (for a  $Ni^{II}$  ion in a regular octahedral environment).

### Description of the Crystal Structures of Complexes **4**, **5**, and **6**

To unambiguously confirm the formulation of the complexes and the coordination mode of the sulfonates and co-ligands X-ray diffraction studies were carried out. Single-crystals of **4**·0.5MeCN·0.5H<sub>2</sub>O, **5**·H<sub>2</sub>O, and **6**·MeCN were obtained from a mixed MeOH/MeCN solution by slow evaporation. All crystal structures consist of discrete  $[Ni_2(L2)(CN_4R)]^+$  cations, tetraphenylborate anions, and solvate molecules of the crystallization medium. Ortep plots of the molecular structures of the cations in **4–6** are depicted in Figure 1, Figure 2, and Figure 3.<sup>[14]</sup> Selected bond lengths and angles are summarized in Table 2 and Table 3. Structural parameters of **1–3** are also included in Table 2 and Table 3 for comparative purposes.<sup>[4]</sup>

The six dinickel(II) complexes in **1–6** share a common structural motif, where the dinickel(II) complex fragments

**Table 1.** Selected IR and UV/Vis analytical data for compounds **4–6**.

Compound	IR bands / $cm^{-1}$	UV/Vis $\lambda_{max}$ /nm ( $\epsilon / M^{-1} cm^{-1}$ )
<b>4</b>	1201 $\nu_s(RSO_3^-)$	443 (19), 624 (14), 1030 (9)
<b>5</b>	1204 $\nu_s(RSO_3^-)$	442 (15), 630 (16), 1030 (11)
<b>6</b>	1203 $\nu_s(RSO_3^-)$	441 (19), 629 (17), 1030 (11)

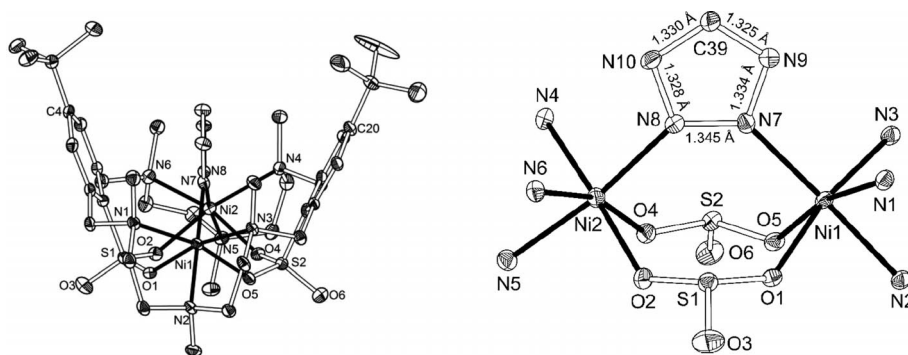


**Figure 1.** Structure of the  $[Ni_2(L2)(CN_4H)]^+$  cation (left) and its core structure (right) in crystals of **4**·0.5MeCN·0.5H<sub>2</sub>O with thermal ellipsoids drawn at 25% probability. Hydrogen atoms are omitted for clarity.

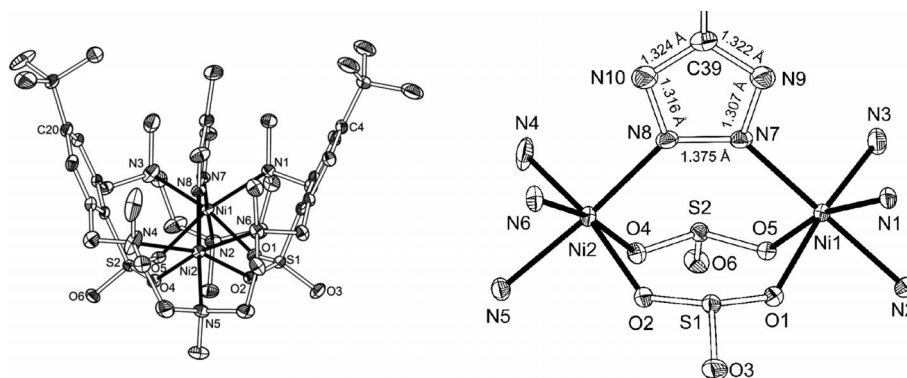


**Figure 2.** Structure of the  $[\text{Ni}_2(\text{L}2)(\text{CN}_4\text{CH}_3)]^+$  cation (left) and its core structure (right) in crystals of  $5 \cdot \text{H}_2\text{O}$  with thermal ellipsoids drawn at 25% probability. Hydrogen atoms (and the Me group bonded to C39 in the right figure) are omitted for clarity.

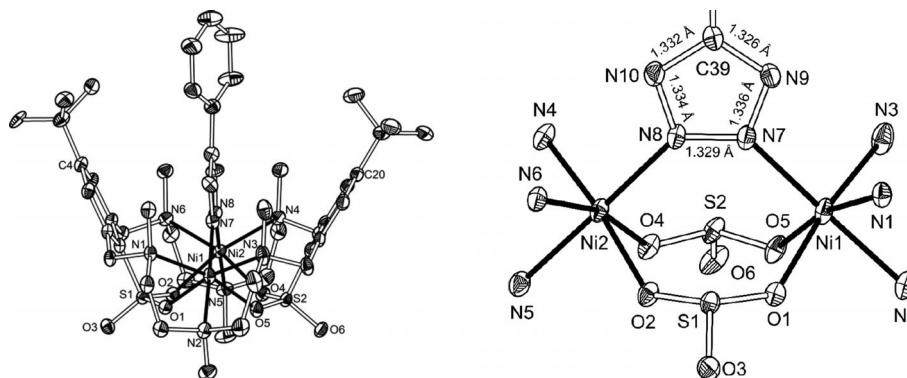


**Figure 3.** Structure of the  $[\text{Ni}_2(\text{L}2)(\text{CN}_4\text{Ph})]^+$  cation (left) and its core structure (right) in crystals of  $6 \cdot \text{MeCN}$  with thermal ellipsoids drawn at 25% probability. Hydrogen atoms (and the Ph ring bonded to C39 in the right figure) are omitted for clarity.

**Table 2.** Selected bond lengths / Å of the complex cations in **1–6**.

X, Y <sup>b)</sup>	<b>1</b> N7, N8	<b>2</b> N7, N8	<b>3A</b> <sup>a)</sup> N7A,N8A	<b>3B</b> N7B,N8B	X, Y <sup>b)</sup>	<b>4A</b> <sup>a)</sup> N7A, N8A	<b>4B</b> N7B, N8B	<b>5</b> N7, N8	<b>6</b> N7,N8
Ni1–X	2.081(2)	2.063(2)	2.071(3)	2.065(3)	Ni1–X	2.080(3)	2.079(3)	2.091(3)	2.0725(18)
Ni1–N1	2.319(2)	2.306(2)	2.346(3)	2.317(3)	Ni1–N1	2.251(3)	2.317(3)	2.272(2)	2.2731(18)
Ni1–N2	2.168(2)	2.162(3)	2.171(3)	2.159(3)	Ni1–N2	2.102(3)	2.128(3)	2.123(2)	2.1142(19)
Ni1–N3	2.227(2)	2.232(3)	2.207(3)	2.221(3)	Ni1–N3	2.237(2)	2.230(3)	2.206(3)	2.231(2)
Ni1–S1	2.5152(7)	2.5044(8)	2.525(1)	[2.532(1)]	Ni1–O1	2.071(2)	2.072(2)	2.069(2)	2.0658(16)
Ni1–S2	2.4626(7)	2.4664(8)	2.431(1)	2.443(1)	Ni1–O5	2.084(2)	2.087(2)	2.093(2)	2.0822(17)
Ni2–Y	2.077(2)	2.071(2)	2.051(3)	2.055(3)	Ni2–Y	2.061(3)	2.072(3)	2.066(3)	2.0802(19)
Ni2–N4	2.237(2)	2.204(2)	2.205(3)	2.210(3)	Ni2–N4	2.394(3)	2.302(3)	2.250(3)	2.236(2)
Ni2–N5	2.173(2)	2.170(2)	2.150(3)	2.154(3)	Ni2–N5	2.112(3)	2.120(3)	2.112(3)	2.125(2)
Ni2–N6	2.311(2)	2.324(2)	2.332(3)	2.338(3)	Ni2–N6	2.254(3)	2.223(4)	2.322(2)	2.2387(18)
Ni2–S1	2.5194(9)	2.5012(8)	2.530(1)	2.515(1)	Ni2–O2	2.085(2)	2.097(2)	2.0645(19)	2.0756(15)
Ni2–S2	2.4509(6)	2.4699(8)	2.450(1)	2.441(1)	Ni2–O4	2.066(2)	2.048(3)	2.0936(19)	2.0580(14)
Ni–N <sup>c)</sup>	2.239(2)	2.233(2)	2.235(3)	2.233(3)	Ni–N <sup>c)</sup>	2.225(3)	2.220(3)	2.214(3)	2.203(2)
Ni–N <sup>d)</sup>	2.079(2)	2.067(2)	2.061(3)	2.060(3)	Ni–N <sup>d)</sup>	2.071(3)	2.076(3)	2.079(3)	2.076(2)
Ni–O <sup>c)</sup>	–	–	–	–	Ni–O <sup>c)</sup>	2.077(2)	2.076(2)	2.080(2)	2.071(2)
Ni–S <sup>c)</sup>	2.4870(8)	2.4855(8)	2.484(1)	2.483(1)	Ni–S <sup>c)</sup>	–	–	–	–
C(4)···C(20)	9.4142(38)	9.2361(50)	9.2952(57)	9.2915(65)	C(4)···C(20)	8.1634(45)	8.1595(61)	8.1838(41)	8.5895(34)
Ni···Ni	3.455(1)	3.425(1)	3.443(1)	3.450(1)	Ni···Ni	4.2796(5)	4.3375(6)	4.3402(6)	4.2607(4)
N7–N8	1.367(2)	1.331(3)	1.346(4)	1.360(4)	N7–N8	1.345(3)	1.358(4)	1.375(4)	1.329(2)
N7–N9	1.325(2)	1.330(3)	1.333(4)	1.320(4)	N7–N9	1.334(4)	1.327(4)	1.307(4)	1.336(3)
N8–N10	1.317(2)	1.335(3)	1.328(4)	1.317(4)	N8–N10	1.328(4)	1.335(4)	1.316(4)	1.334(3)
C39–N9	1.331(3)	1.333(4)	1.341(5)	1.347(5)	C39–N9	1.325(5)	1.326(4)	1.322(4)	1.326(3)
C39–N10	1.341(3)	1.333(4)	1.347(5)	1.354(5)	C39–N10	1.330(4)	1.326(5)	1.325(5)	1.332(3)

a) There are two crystallographically independent molecules A and B in the unit cell. b) X and Y denote the donor atoms of the coligands. c) Average values. d) Average Ni–N heterocycle distance.

**Table 3.** Selected bond angles  $^\circ$  of the complex cations in **1–6**.

X, Y <sup>b)</sup>	<b>1</b> N7, N8	<b>2</b> N7, N8	<b>3A<sup>a)</sup></b> N7A, N8A	<b>3B<sup>a)</sup></b> N7B, N8B	X, Y <sup>b)</sup>	<b>4A<sup>a)</sup></b> N7A, N8A	<b>4B<sup>a)</sup></b> N7B, N8B	<b>5</b> N7, N8	<b>6</b> N7, N8
X–Ni1–N2	175.18(7)	176.67(9)	175.05(12)	175.52(11)	X–Ni1–N2	178.34(11)	172.46(12)	178.57(10)	177.89(8)
N1–Ni1–S2	169.73(5)	169.12(7)	167.52(8)	169.09(8)	O5–Ni1–N1	167.42(9)	170.25(10)	167.05(9)	167.64(7)
N3–Ni1–S1	170.64(4)	171.60(7)	171.91(9)	171.21(8)	O1–Ni1–N3	167.95(9)	163.31(10)	167.68(11)	168.22(8)
X–Ni1–S1	85.27(5)	85.25(7)	83.92(9)	84.43(8)	X–Ni1–O1	94.04(9)	93.59(10)	92.81(9)	95.39(7)
X–Ni1–S2	87.12(5)	87.78(6)	87.88(9)	87.29(9)	X–Ni1–O5	93.88(10)	91.94(10)	94.18(8)	95.36(7)
X–Ni1–N3	94.45(7)	96.46(10)	94.45(12)	96.17(11)	X–Ni1–N3	96.68(10)	97.87(10)	96.15(10)	93.89(8)
X–Ni1–N1	96.21(6)	96.33(9)	97.11(11)	95.87(11)	X–Ni1–N1	96.29(10)	91.98(10)	95.54(9)	93.97(7)
N1–Ni1–N3	98.48(6)	97.98(9)	99.03(11)	98.19(11)	N1–Ni1–N3	99.80(9)	109.00(11)	102.93(10)	101.75(8)
N1–Ni1–S1	90.85(5)	89.98(6)	89.04(8)	90.46(8)	O1–Ni1–N1	84.44(9)	82.57(9)	84.54(8)	84.85(6)
N2–Ni1–N1	80.23(6)	80.96(9)	79.35(12)	80.52(11)	N2–Ni1–N1	84.64(10)	80.95(11)	83.03(10)	83.92(7)
N2–Ni1–S1	97.97(6)	96.64(8)	99.40(9)	98.20(8)	O1–Ni1–N2	84.67(9)	88.10(10)	86.93(9)	84.62(7)
N2–Ni1–N3	82.93(7)	82.07(10)	82.77(12)	81.79(11)	N2–Ni1–N3	84.51(10)	82.12(10)	84.32(10)	86.38(8)
N2–Ni1–S2	96.95(5)	95.23(7)	96.29(9)	96.74(8)	O5–Ni1–N2	85.03(10)	95.46(10)	87.22(9)	86.75(7)
N3–Ni1–S2	90.92(5)	91.54(6)	91.95(9)	91.82(8)	O5–Ni1–N3	86.31(9)	79.28(11)	84.49(10)	85.69(8)
S1–Ni1–S2	79.72(3)	80.30(3)	80.08(3)	79.43(3)	O5–Ni1–O1	87.49(8)	88.27(10)	86.45(8)	86.22(6)
Y–Ni2–N5	175.33(6)	175.39(9)	175.56(12)	175.05(12)	Y–Ni2–N5	171.39(11)	178.56(13)	174.48(10)	178.68(8)
N4–Ni2–S1	171.30(4)	171.00(7)	171.28(9)	171.66(8)	O2–Ni2–N4	169.94(9)	167.36(11)	163.12(12)	167.47(6)
N6–Ni2–S2	169.16(4)	168.47(6)	169.34(8)	168.92(8)	O4–Ni2–N6	164.05(9)	167.70(12)	169.02(9)	165.61(7)
Y–Ni2–S1	85.13(5)	84.53(6)	85.07(9)	84.73(9)	Y–Ni2–O2	94.30(9)	93.74(10)	93.68(9)	94.94(7)
Y–Ni2–S2	86.86(5)	87.61(7)	86.56(9)	87.19(9)	Y–Ni2–O4	93.59(10)	93.59(11)	93.18(9)	95.87(7)
Y–Ni2–N4	95.69(6)	95.20(9)	96.14(12)	95.18(12)	Y–Ni2–N4	90.63(10)	95.01(11)	97.32(11)	93.71(8)
Y–Ni2–N6	96.17(6)	97.02(9)	95.55(12)	96.15(11)	Y–Ni2–N6	98.48(10)	96.74(12)	93.39(9)	95.87(7)
N4–Ni2–S2	91.53(5)	90.70(7)	91.81(9)	91.86(8)	O4–Ni2–N4	79.86(9)	84.40(10)	79.47(10)	84.50(6)
N6–Ni2–S1	90.01(4)	89.61(6)	90.13(8)	89.96(8)	O2–Ni2–N6	77.71(10)	86.71(11)	83.61(8)	85.11(6)
N5–Ni2–S1	98.04(4)	98.43(7)	97.23(9)	98.11(9)	O2–Ni2–N5	94.19(10)	87.35(10)	88.35(9)	86.34(7)
N5–Ni2–S2	97.04(5)	96.35(7)	97.59(9)	97.29(9)	O4–Ni2–N5	87.67(10)	85.55(12)	92.05(9)	83.89(7)
N5–Ni2–N4	81.69(6)	82.43(9)	82.17(12)	82.59(12)	N5–Ni2–N4	81.20(10)	83.77(11)	81.89(11)	84.98(8)
N5–Ni2–N6	80.46(6)	79.53(9)	80.67(12)	79.85(11)	N5–Ni2–N6	81.96(10)	84.24(13)	81.72(9)	84.55(7)
N4–Ni2–N6	98.50(6)	99.35(9)	98.33(11)	98.33(11)	N6–Ni2–N4	110.25(10)	101.28(12)	108.37(10)	103.00(7)
S1–Ni2–S2	79.86(2)	80.29(3)	79.63(3)	79.80(3)	O2–Ni2–O4	91.06(9)	85.97(10)	87.19(8)	85.61(6)
Ni1–S1–Ni2	86.68(3)	86.36(3)	85.87(4)	86.23(3)	Ni1–S1–Ni2	–	–	–	–
Ni1–S2–Ni2	89.378(2)	87.88(3)	89.74(4)	89.86(3)	Ni1–S2–Ni2	–	–	–	–
Ph/Ph <sup>c)</sup>	82.655(58)	77.998(82)	79.774(111)	80.507(120)	Ph/Ph <sup>c)</sup>	47.782(97)	47.827(110)	48.924(84)	56.547(72)

a) There are two crystallographically independent molecules A and B in the unit cell. b) X and Y denote the donor atoms of the coligands. c) Angle between the normals of the planes of the aryl rings.

$[Ni_2(L_2)]^{2+}$  and  $[Ni_2(L_1)]^{2+}$  adopt a conical “calixarene-like” conformation that gives rise to a hydrophobic cavity.<sup>[15]</sup> In each case the two nickel(II) ions are coordinated in a square-pyramidal fashion either by a *fac*- $N_3(\mu\text{-S})_2$  {in  $[Ni_2(L_1)]^{2+}$ } or a *fac*- $N_3O_2$  donorset {in  $[Ni_2(L_2)]^{2+}$ }. Together with the  $\mu_{2,3}$ -bridging tetrazolato coligands each of the nickel(II) atoms reaches a distorted octahedral coordination environment. In all cases the tetrazolate units are effectively planar and bridge the Ni<sup>II</sup> ions in a symmetrical fashion through their two ring nitrogen atoms N(7) and N(8). With 2.060(3)–2.079(3) Å the average Ni–N<sup>het</sup> bond length is very similar in all six complexes. The N–N and C–N bond lengths of the coordinated tetrazolates however differ significantly from those of the free tetrazoles. This is in agreement with the fact that upon removal of the proton the nitrogen atoms N7, N8 and N9, N10 become equivalent.<sup>[16]</sup> It can be noted that the N(7)–N(8) bonds in **4–6** show an average bond length of 1.352(3) Å, which is much longer than the 1.295(3) Å and 1.285(3) Å found in 1-H-tetrazole and 5-methyltetrazole.<sup>[17,18]</sup> As one might expect the Ni<sup>II</sup>–Ni<sup>II</sup> distances in the oxidized complexes are significantly longer (0.81–0.91 Å) than the corresponding distances in their reduced counterparts in order to accommodate the coordinating sulfonate oxygen atoms. That of course leads to drastic

changes in the shape of the cavity.<sup>[7,8]</sup> These changes can be expressed by the intramolecular distance between the two aryl carbon atoms C(4) and C(20) and the angle between the normals of the planes that are generated by the phenyl rings of the macrocycle. While the angles between the Ph rings in **1–3** are all greater than 77°, the corresponding values in **4–6** are all significantly smaller (below 57°). The C(4)–C(20) distances are thus shortened by 0.7–1.3 Å, a fact that results in a more “cleft”-like rather than a “cone”-like binding pocket.

### Magnetic Measurements

To examine their electronic structures, measurements of the temperature dependent magnetic susceptibility of the sulfonato complexes **4–6** were carried out on powdered samples at an applied external field of 0.5 T in the temperature range between 2 and 330 K with a MPMS 7XL SQUID (Quantum Design) magnetometer. The temperature dependencies of the molar magnetic susceptibility (per dinuclear complex) of the complexes **4–6** are shown in Figure 4 in the form of  $\chi_M T$  vs.  $T$  plots. The susceptibility data of their parent complexes **1–3** are shown for comparative purposes.<sup>[3]</sup>

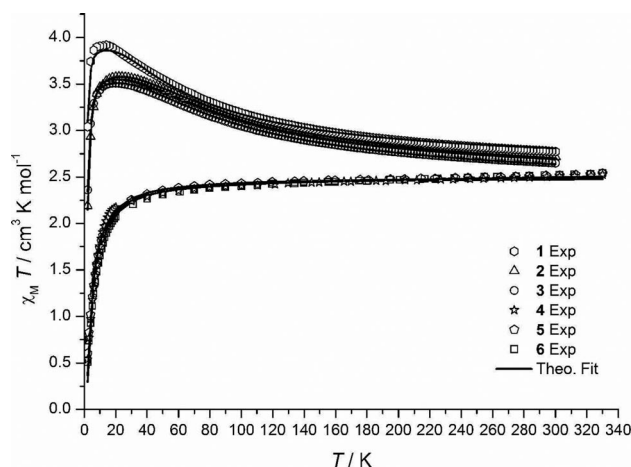


**Figure 4.** The temperature dependencies of the molar magnetic susceptibility (per dinuclear complex) of the complexes **4–6** and their parent complexes **1–3**<sup>[3]</sup> in the form of  $\chi_M T$  vs.  $T$  plots. The full lines represent the best theoretical fits to Equation (1).

The  $\chi_M T$  values of **4** slowly decrease from  $2.53 \text{ cm}^3 \cdot \text{K} \cdot \text{mol}^{-1}$  ( $4.49 \mu_B$ ) at 330 K to  $0.54 \text{ cm}^3 \cdot \text{K} \cdot \text{mol}^{-1}$  ( $2.08 \mu_B$ ) at 2 K. This is in contrast to **1**, where the values increase with decreasing temperature from  $2.77 \text{ cm}^3 \cdot \text{K} \cdot \text{mol}^{-1}$  ( $4.71 \mu_B$ ) at 300 K to a maximum of  $3.92 \text{ cm}^3 \cdot \text{K} \cdot \text{mol}^{-1}$  ( $5.60 \mu_B$ ) at 14 K. A similar behavior can be noted for the other two complex pairs **2/5** and **3/6**. Thus, for **5** the  $\chi_M T$  data decreases from  $2.54 \text{ cm}^3 \cdot \text{K} \cdot \text{mol}^{-1}$  ( $4.51 \mu_B$ ) at 330 K to  $0.60 \text{ cm}^3 \cdot \text{K} \cdot \text{mol}^{-1}$  ( $2.20 \mu_B$ ) at 2 K. In the parent complex **2** the product  $\chi_M T$  gradually increases from  $2.71 \text{ cm}^3 \cdot \text{K} \cdot \text{mol}^{-1}$  ( $4.66 \mu_B$ ) at 300 K to a maximum of  $3.58 \text{ cm}^3 \cdot \text{K} \cdot \text{mol}^{-1}$  ( $5.35 \mu_B$ ) at 22 K. Further lowering of the temperature is accompanied by a rapid decrease of  $\chi_M T$ , being  $2.19 \text{ cm}^3 \cdot \text{K} \cdot \text{mol}^{-1}$  ( $4.18 \mu_B$ ) at 2 K. Again, for **6** the  $\chi_M T$  values decrease from  $2.54 \text{ cm}^3 \cdot \text{K} \cdot \text{mol}^{-1}$  ( $4.51 \mu_B$ ) at 330 K to  $0.51 \text{ cm}^3 \cdot \text{K} \cdot \text{mol}^{-1}$  ( $2.02 \mu_B$ ) at 2 K. For **3**, on the other hand, the product  $\chi_M T$  gradually increases again from  $2.65 \text{ cm}^3 \cdot \text{K} \cdot \text{mol}^{-1}$  ( $4.60 \mu_B$ ) at 300 K to a maximum of  $3.51 \text{ cm}^3 \cdot \text{K} \cdot \text{mol}^{-1}$  ( $5.30 \mu_B$ ) at 22 K. Further decrease in temperature is accompanied by a rapid decrease of  $\chi_M T$ , being  $2.36 \text{ cm}^3 \cdot \text{K} \cdot \text{mol}^{-1}$  ( $4.35 \mu_B$ ) at 2 K. Thus oxidation of the thiophenolato complexes is in all cases accompanied by a change of the exchange coupling between the electron spins of the Ni<sup>II</sup> ions from ferromagnetic in **1–3** to antiferromagnetic in **4–6**. Thus, **4–6** exhibit an  $S = 0$  spin ground state and **1–3** have an  $S = 2$  spin ground state. Since the coligands are chemi-

cally very similar it can be concluded that this difference solely originates from the oxidation of the supporting ligand.

In order to quantify the magnitude of the magnetic exchange interaction and to determine the  $g$  values of the complexes **4–6** the experimental  $\chi_M T$  vs.  $T$  data were analyzed using the spin Hamiltonian [Equation (1)], including the isotropic Heisenberg-Dirac-van-Vleck (HDvV) exchange, the single-ion zero-field splitting and the single-ion Zeeman interactions using a full-matrix diagonalization approach.<sup>[19,20]</sup>

$$H = -2J\hat{S}_1\hat{S}_2 + \sum_{i=1}^2 \left[ D_i(\hat{S}_{zi}^2 - \frac{1}{3}\hat{S}_i(\hat{S}_i + 1)) + g_i\mu_B\hat{S}_{iz}B_z \right] \quad (\tau = x, y, z) \quad (1)$$

The experimental data of **4–6** were fitted to Equation (1) over the full temperature range, assuming identical  $g$  values for the two Ni<sup>II</sup> ions. The parameters of **4–6** leading to the best fits are listed in Table 4 together with the parameters determined earlier for **1–3**.<sup>[3]</sup> The parameters determined for **4** were  $J = -1.39 \text{ cm}^{-1}$  and  $g = 2.22$ . In the case of **5** the best fit to the experimental data yielded  $J = -1.43 \text{ cm}^{-1}$  and  $g = 2.24$ . The best fit parameters for **6** were  $J = -1.60 \text{ cm}^{-1}$  and  $g = 2.26$ . In the case of **1–3** the inclusion of the zero-field splitting parameter improved the quality of the fit. In the case of **4–6**, however, the fit was found to be quite insensitive to the value of  $D$ . Therefore  $D$  was fixed to zero in this case. It should be mentioned in this respect that magnetic susceptibility measurements are not very suitable for the determination of the  $D$  parameter,<sup>[21]</sup> and so these values should be taken indicative than definite. A previous high-field EPR study has shown that the  $D$  values for Ni<sup>II</sup><sub>2</sub> complexes supported by the N<sub>6</sub>S<sub>2</sub> macrocycle have a negative sign and are on the order of  $0.5\text{--}1.0 \text{ cm}^{-1}$ .<sup>[22]</sup> Nevertheless, the value of  $J$  is unambiguous and represents an accurate measure of the magnetic coupling in these complexes.

The change of the sign of  $J$  is presumably associated with a change of the angle between the magnetic orbitals of the two Ni<sup>II</sup> ions. It should be noted in this respect that there is a large increase of the angle between the N<sub>2</sub>NiS<sub>2</sub> and N<sub>2</sub>Ni(O<sup>sulfonato</sup>)<sub>2</sub> planes upon going from the thiophenolato-bridged compounds **1–3** to the sulfonato-bridged species **4–6**. Thus, the angles between the normals of the planes through the S<sub>1</sub>S<sub>2</sub>N<sub>6</sub>N<sub>4</sub> and S<sub>1</sub>S<sub>2</sub>N<sub>1</sub>N<sub>3</sub> planes in the former are all  $< 48^\circ$  (**1**:  $46.87(3)^\circ$ , **2**:  $46.67(4)^\circ$ , **3**:  $47.16(6)^\circ$  [ $47.14(5)^\circ$ ]), whereas the angles between the normals of the planes through the O<sub>4</sub>O<sub>2</sub>N<sub>6</sub>N<sub>4</sub> and O<sub>5</sub>O<sub>1</sub>N<sub>1</sub>N<sub>3</sub> planes in the latter series are all at  $> 87^\circ$  (**4**:  $87.71(5)^\circ$  [ $88.57(7)^\circ$ ], **5**:  $87.56(6)^\circ$ , **6**:  $89.35(4)^\circ$ ). Further it

**Table 4.** Magnetic parameters for **1–6** resulting from analysis of temperature dependent magnetic susceptibility data and from DFT calculations.

Complex	$J^a$ /cm <sup>-1</sup>	$g^a$	$D^a$ /cm <sup>-1</sup>	$J(1)^c$ /cm <sup>-1</sup>	$J(2)^c$ /cm <sup>-1</sup>	$J(3)^c$ /cm <sup>-1</sup>
	Exp.	Exp.	Exp	B3LYP	B3LYP	B3LYP
<b>1</b>	+13.50 <sup>b)</sup>	2.28 <sup>b)</sup>	0.98 <sup>b)</sup>	28.38	18.92	28.36
<b>2</b>	+20.00 <sup>b)</sup>	2.20 <sup>b)</sup>	8.10 <sup>b)</sup>	26.03	17.35	26.02
<b>3</b>	+19.20 <sup>b)</sup>	2.17 <sup>b)</sup>	5.85 <sup>b)</sup>	27.71	18.47	27.70
<b>4</b>	-1.39	2.22	0 (fixed)	-2.84	-1.89	-2.84
<b>5</b>	-1.43	2.24	0 (fixed)	-2.39	-1.59	-2.39
<b>6</b>	-1.60	2.26	0 (fixed)	-2.94	-1.96	-2.94

a) Parameters resultant from least-squares fit to the  $\chi_M T$  data under the spin Hamiltonian in Equation (1),  $J$  = coupling constant ( $H = -2JS_1S_2$ ),  $g = g$  value,  $D$  = zero-field-splitting parameter. b) Parameters from Ref. [3]. c) Parameters obtained from calculations with the ORCA program.

can be noted that the absolute value of the exchange interaction in **4–6** compared to that in **1–3** is smaller by an order of magnitude. This observation may be explained with the increased Ni⋯Ni distance and therefore increased length of the coupling path upon oxidation.

### Theoretical Calculations

The results of the DFT calculations for **1–6** are summarized in Table 4. As shown by Equation (2), Equation (3), and Equation (4), there are three formulations available for the evaluation of the magnetic coupling constants.<sup>[23–27]</sup>

$$J(1) = \frac{E^{\text{BS}} - E^{\text{HS}}}{S_{\text{max}}^2} \quad (2)$$

$$J(2) = \frac{E^{\text{BS}} - E^{\text{HS}}}{S_{\text{max}} \cdot (S_{\text{max}} + 1)} \quad (3)$$

$$J(3) = \frac{E^{\text{BS}} - E^{\text{HS}}}{\langle S^2 \rangle^{\text{HS}} - \langle S^2 \rangle^{\text{BS}}} \quad (4)$$

Herein, the formulations according to Noodleman,  $J(1)$ <sup>[23–25]</sup> and  $J(2)$ <sup>[26]</sup> are valid for weak and strong coupling, respectively, whereas  $J(3)$  as published by Yamaguchi et al.<sup>[27]</sup> holds for the whole range of coupling strengths and reduces to  $J(1)$  or  $J(2)$ , respectively, in either of the edge cases.<sup>[28]</sup> Regardless of the chosen formulation, the calculations reproduce the correct sign of  $J$ . The experimental exchange coupling constants seem to be very closely resembled by the DFT calculations using the formulation  $J(2)$  by Bencini. Nevertheless, assuming the formulation according to Yamaguchi et al. [ $J(3)$ ] to be the most reasonable, it turns out that the calculated coupling constants overestimate the magnitude as compared to experi-

mental data. This is in agreement with a study of Soda and co-workers who found the B3LYP functional to overestimate coupling constants especially at incomplete basis sets. Furthermore, the observed numbers of  $J(1)$  and  $J(3)$  do not differ significantly, as is predicted to be the case for weak coupling as present in the investigated complexes.

The observation of ferromagnetic exchange interactions in **1–3**, for which the Ni–S–Ni angles are close 90° is in good agreement with earlier studies,<sup>[3,29]</sup> and accords to the Anderson<sup>[30,31]</sup> and Goodenough-Kanamori rules.<sup>[32–34]</sup> The occurrence of antiferromagnetic coupling in **4–6** is caused by the alteration of the electronic structure of the complexes upon the change of the coordination sphere around each Ni<sup>II</sup> ion from  $N_4S_2$  to  $N_4O_2$ . Due to the replacement of the soft sulfur donor atoms by hard oxygen atoms the degeneracy of the magnetic orbitals is lost and the antiferromagnetic singlet term is stabilized.<sup>[20]</sup> The observed antiferromagnetic behavior is in accordance with the Hay-Thibeault-Hoffmann model<sup>[35]</sup> and fits the results given in the literature.<sup>[8]</sup> As illustrated for **1** and **4** in Figure 5 the difference of alpha and beta electron density of complexes **1–6** shows positive values indicating an excess of alpha electrons at the nickel atoms. Interestingly, for **1–3** coupling of these electrons is mediated mainly across the sulfur atoms leading to ferromagnetic coupling (90° Ni–S–Ni angle), while for **4–6** an antiferromagnetic coupling pathway is mediated mainly via the bridging tetrazolato coligands. Graphical representations of the coupling pathways and spin densities of the other compounds are available as Supporting Information.

### Conclusions

The oxidation of dinuclear nickel complexes  $[Ni_2(L)(L')]BPh_4$  [ $L' = CN_4H^-$  (**1**),  $CN_4Me^-$  (**2**), and  $CN_4Ph^-$  (**3**)] supported by the hexaaza bis(thiophenolate) ligand  $(L1)^{2-}$

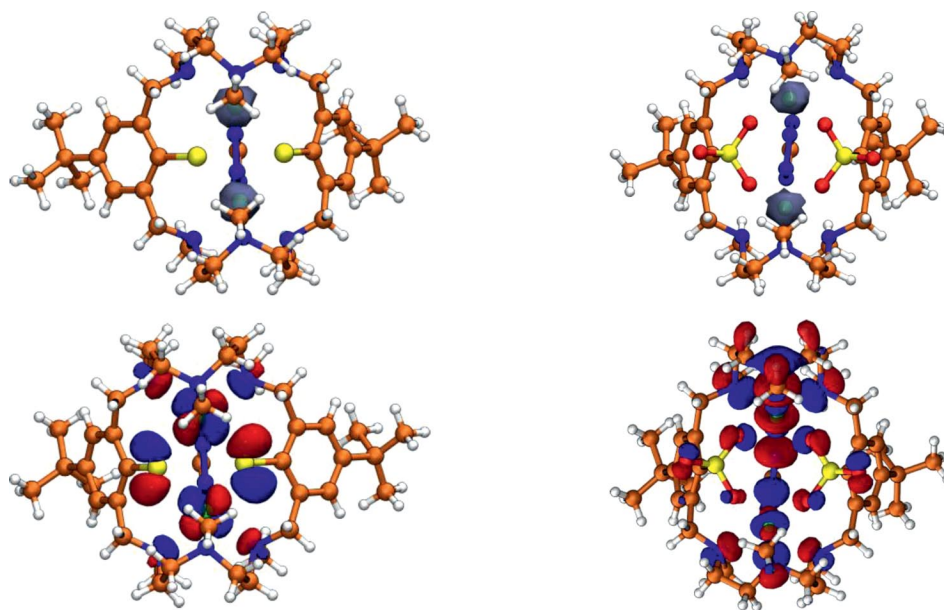


**Figure 5.** Top: Graphical representation of the spin densities of compounds **1** (left) and **4** (right) at an isovalue of 0.025. Bottom: Ferromagnetic coupling pathway across the sulfur atoms in **1** (left) and antiferromagnetic coupling pathway across the bridging coligand in **4** (right).

with H<sub>2</sub>O<sub>2</sub> produces the corresponding complexes **4–6** of the disulfonate macrocycle [Ni<sub>2</sub>(L<sub>2</sub>)(L')]<sub>2</sub>BPh<sub>4</sub>. While the overall structures of the complexes remain constant, the magnetic properties change significantly. Upon oxidation the intramolecular magnetic exchange interaction between the electron spins of the Ni<sup>II</sup> ions changes from ferromagnetic to antiferromagnetic due to replacement of a bridging thiophenolate to a bridging sulfonate moiety in the coupling path. The magnetic properties, however, were not markedly influenced by the size of the functional group *R* of the 5-*R*-tetrazolates. The *J* values that were obtained by DFT calculations are in good agreement with the experimentally determined values. The calculations also shed light on the way the magnetic exchange interactions are propagated between the two metal atoms in the two complex types.

## Experimental Section

**General Remarks:** Solvents and reagents were of reagent grade quality and used as received unless otherwise specified. Infrared spectra were recorded with a Bruker Vector 27 FT-IR spectrometer. Electronic absorption spectra were taken with a JASCO V-670 UV/Vis/NIR spectrophotometer, elemental analyses with a VARIO EL – elemental analyzer. Temperature-dependent magnetic susceptibility measurements on powdered solid samples were carried out with a MPMS 7XL SQUID magnetometer (Quantum Design). The observed susceptibility data were corrected for underlying diamagnetism.

**[Ni<sub>2</sub>(L<sub>2</sub>)(CN<sub>4</sub>H)]BPh<sub>4</sub> (**4**):** To a solution of [Ni<sub>2</sub>(L<sub>1</sub>)(CN<sub>4</sub>H)]BPh<sub>4</sub> (**1**) (100 mg, 0.09 mmol) in methanol (60 mL) was added hydrogen peroxide (2 mL, 50 wt% solution in water, 35.19 mmol). Refluxing the reaction mixture for 10 h yielded a pale green solution. After cooling to room temperature the solution was filtered, and a solution of NaBPh<sub>4</sub> (146 mg, 0.43 mmol) in ethanol (10 mL) was added to the filtrate. The amount of solvent was reduced to about 10 mL under reduced pressure to precipitate the pale-green microcrystalline tetraphenylborate salt **4**, which was isolated by filtration, thoroughly washed with cold ethanol and dried in vacuo. Yield: 73 mg (0.06 mmol, 67%). C<sub>63</sub>H<sub>85</sub>BN<sub>10</sub>Ni<sub>2</sub>O<sub>6</sub>S<sub>2</sub> (1270.74): calcd. C 59.55, H 6.74, N 11.02%; found C 59.57, H 6.84, N 11.11%. IR (KBr):  $\tilde{\nu}$  = 3448 (m), 3054 (w), 3031 (w), 2999 (w), 2982 (w), 2964 (s), 2906 (w), 2868 (m), 1631 (w), 1601 (m), 1581 (w), 1478 (s), 1429 (w), 1411 (w), 1396 (w), 1367 (m), 1309 (w), 1301 (w), 1270 (w), 1258 (w), 1241 (w), 1201 (s), 1157 (w), 1091 (s), 1062 (w), 1044 (w), 1031 (m), 1016 (w), 1007 (w), 976 (w), 916 (w), 890 (m), 851 (w), 832 (w), 821 (m), 802 (w), 744 (w), 734 (s), 711 (w), 705 (s), 668 (m), 640 (w), 629 (w), 614 (w), 606 (m), 596 (w), 561 (w), 548 (w) cm<sup>-1</sup>. ESI-MS<sup>+</sup> (MeCN): *m/z* = 949.20 [C<sub>39</sub>H<sub>65</sub>N<sub>10</sub>Ni<sub>2</sub>O<sub>6</sub>S<sub>2</sub>]<sup>+</sup>. UV/Vis (CH<sub>3</sub>CN):  $\lambda_{\text{max}}$  ( $\epsilon$ , M<sup>-1</sup> cm<sup>-1</sup>) = 383 (38), 443 (19), 624 (14), 1030 (9) nm.

**[Ni<sub>2</sub>(L<sub>2</sub>)(CN<sub>4</sub>Me)]BPh<sub>4</sub> (**5**):** This compound was prepared from [Ni<sub>2</sub>(L<sub>1</sub>)(CN<sub>4</sub>Me)]<sub>2</sub>BPh<sub>4</sub> (**2**) (100 mg, 0.08 mmol) in a manner analogous to **4**. Yield: 68 mg (0.05 mmol, 63%). C<sub>64</sub>H<sub>87</sub>BN<sub>10</sub>Ni<sub>2</sub>O<sub>6</sub>S<sub>2</sub> (1284.77) calcd. C 59.83; H 6.83; N 10.90%; found C 58.86, H 6.96, N 10.40%. IR (KBr):  $\tilde{\nu}$  = 3597 (w), 3379 (w), 3057 (w), 3039 (w), 3002 (w), 2968 (m), 2869 (w), 1602 (w), 1581 (w), 1480 (s), 1428 (w), 1412 (w), 1397 (w), 1367 (w), 1270 (w), 1231 (w), 1204 (s), 1151 (w), 1091 (m), 1060 (w), 1045 (w), 1032 (m), 1002 (w), 978 (w), 916 (w), 893 (m), 821 (m), 803 (w), 741 (m), 735 (w), 709 (s), 668 (m), 639 (w), 631 (w), 611 (m), 597 (w), 562 (w), 548 (w) cm<sup>-1</sup>. ESI-MS<sup>+</sup> (MeCN): *m/z* = 963.34 [C<sub>40</sub>H<sub>67</sub>N<sub>10</sub>Ni<sub>2</sub>O<sub>6</sub>S<sub>2</sub>]<sup>+</sup>. UV/Vis (CH<sub>3</sub>CN):  $\lambda_{\text{max}}$  ( $\epsilon$ , M<sup>-1</sup> cm<sup>-1</sup>) = 378 (40), 442 (15), 630 (16), 1030 (11) nm.

**[Ni<sub>2</sub>(L<sub>2</sub>)(CN<sub>4</sub>Ph)]BPh<sub>4</sub> (**6**):** This compound was prepared from [Ni<sub>2</sub>(L<sub>1</sub>)(CN<sub>4</sub>Ph)]<sub>2</sub>BPh<sub>4</sub> (**3**) (100 mg, 0.08 mmol) in a manner analogous to **4**. Yield: 69 mg (0.07 mmol, 64%). C<sub>69</sub>H<sub>89</sub>BN<sub>10</sub>Ni<sub>2</sub>O<sub>6</sub>S<sub>2</sub> (1346.84): calcd. C 61.53; H 6.66; N 10.40%; found C 60.76, H 6.66, N 10.09%. IR (KBr):  $\tilde{\nu}$  = 3455 (m), 3055 (w), 3032 (w), 2999 (w), 2964 (s), 2869 (w), 1601 (m), 1580 (w), 1478 (w), 1450 (s), 1429 (w), 1411 (w), 1397 (w), 1366 (m), 1268 (w), 1250 (w), 1203 (s), 1150 (w), 1132 (w), 1090 (s), 1059 (w), 1043 (w), 1032 (m), 1012 (w), 999 (w), 974 (w), 913 (w), 893 (m), 831 (w), 821 (s), 750 (w), 733 (s), 705 (s), 667 (s), 640 (w), 630 (m), 612 (m), 598 (w), 562 (w), 548 (w) cm<sup>-1</sup>. ESI-MS<sup>+</sup> (MeCN): *m/z* = 1025.36 [C<sub>45</sub>H<sub>69</sub>N<sub>10</sub>Ni<sub>2</sub>O<sub>6</sub>S<sub>2</sub>]<sup>+</sup>. UV/Vis (CH<sub>3</sub>CN):  $\lambda_{\text{max}}$  ( $\epsilon$ , M<sup>-1</sup> cm<sup>-1</sup>) = 382 (42), 441 (19), 629 (17), 1030 (11) nm.

**Crystal Structure Determinations:** The X-ray diffraction data were collected at 183 K with a IPDS-1T (STOE) or a IPDS-2T (STOE) diffractometer using graphite monochromated Mo-*K*<sub>α</sub> radiation ( $\lambda$  = 0.71073 Å). The intensity data were processed with the program STOE X-Area.<sup>[36]</sup> The crystal structures were solved by direct methods and refined by full-matrix least-squares on the basis of all data against *F*<sup>2</sup> using SHELXL-97.<sup>[37]</sup> Diamond 3.2g was used for the creation of artwork.<sup>[14]</sup> Unless otherwise noted non-hydrogen atoms were refined anisotropically whereas the coordinates of the hydrogen atoms were calculated for idealized positions with isotropic displacement parameters. Selected crystallographic data are tabulated in Table 5.

In the crystal structure of **4**·0.5MeCN·0.5H<sub>2</sub>O the water solvate molecules were refined isotropically. The bond lengths<sup>[38]</sup> of the acetonitrile molecules were constrained to C–C = 1.470 Å and C–N = 1.136 Å using the DFIX command implemented in the SHELXL program suite. Furthermore one of the *tert*-butyl groups was found to be rotationally disordered. The disorder was refined applying a split model using the PART command yielding an occupancy factor of 0.76/0.24. In the crystal structure of **5**·H<sub>2</sub>O one of the *tert*-butyl groups and the atoms C13 and C24 were found to be disordered. The two disorders were found to have similar occupancy factors and a split model with an occupancy factor of 0.68/0.32 was applied. In the crystal structure of **6**·MeCN rotational disorder occurred at one of the *tert*-butyl groups and at the phenyl ring of the coligand. Hence split models had to be applied yielding occupancy factors of 0.57/0.43 and 0.64/0.36 respectively.

Crystallographic data (excluding structure factors) for the structures in this paper have been deposited with the Cambridge Crystallographic Data Centre, CCDC, 12 Union Road, Cambridge CB21EZ, UK. Copies of the data can be obtained free of charge on quoting the depository numbers CCDC-901287 (**4**·0.5MeCN·0.5H<sub>2</sub>O), CCDC-901288 (**5**·H<sub>2</sub>O), and CCDC-901289 (**6**·MeCN) (Fax: +44-1223-336-033; E-Mail: deposit@ccdc.cam.ac.uk, http://www.ccdc.cam.ac.uk).

**Electronic Structure Calculations:** All density functional theory (DFT) calculations were performed applying the Kohn-Sham density functional theory (KS-DFT) in conjunction with the def2-TZVP basis set<sup>[39,40]</sup> using the ORCA program.<sup>[41]</sup> The investigated geometries were obtained from X-ray diffraction studies. No further geometry optimizations were carried out in order to get results resembling the molecular geometry in the crystal structures. We employed the hybrid functional B3LYP.<sup>[42–46]</sup> Coupling constants were evaluated by broken symmetry calculations using the FlipSpin feature of ORCA. Graphical representations of spin density and of the HOMOs and LUMOs were created using the visual molecular dynamics (VMD) software.<sup>[47]</sup>

**Supporting Information** (see footnote on the first page of this article): Experimental and calculated susceptibility data for complexes **1–6** and graphical representations of coupling pathways and spin densities.

**Table 5.** Selected crystallographic data for compounds **4**·0.5MeCN·0.5H<sub>2</sub>O, **5**·H<sub>2</sub>O, and **6**·MeCN.

	<b>4</b> ·0.5MeCN·0.5H <sub>2</sub> O	<b>5</b> ·H <sub>2</sub> O	<b>6</b> ·MeCN
Formula	C <sub>64</sub> H <sub>86.50</sub> BN <sub>10.50</sub> Ni <sub>2</sub> O <sub>6.50</sub> S <sub>2</sub>	C <sub>64</sub> H <sub>87</sub> BN <sub>10</sub> Ni <sub>2</sub> O <sub>7</sub> S <sub>2</sub>	C <sub>71</sub> H <sub>92</sub> BN <sub>11</sub> Ni <sub>2</sub> O <sub>6</sub> S <sub>2</sub>
M /g·mol <sup>-1</sup>	1299.29	1300.79	1387.91
Space group	<i>P</i> 2 <sub>1</sub> / <i>a</i>	<i>C</i> 2/ <i>c</i>	<i>P</i> 2 <sub>1</sub> / <i>c</i>
<i>a</i> /Å	14.2594(5)	21.5600(8)	12.9343(6)
<i>b</i> /Å	50.4554(17)	19.1490(6)	34.3993(9)
<i>c</i> /Å	18.7925(7)	31.3230(12)	15.7358(7)
<i>a</i> /°	90	90	90
<i>β</i> /°	110.670(3)	93.069(5)	97.145(3)
<i>γ</i> /°	90	90	90
<i>V</i> /Å <sup>3</sup>	12650.2(8)	12913.2(8)	6947.0(5)
<i>Z</i>	8	8	4
$\rho_{\text{calcd}}$ /g·cm <sup>-3</sup>	1.364	1.338	1.327
Crystal size /mm <sup>3</sup>	0.18 × 0.14 × 0.11	0.16 × 0.14 × 0.11	0.17 × 0.15 × 0.10
$\mu$ (Mo- <i>K</i> <sub>α</sub> ) /mm <sup>-1</sup>	0.71073	0.71073	0.71073
$\theta$ limits /°	1.2–28.1	2.4–28.1	1.4–27.2
Measured refl.	54592	43988	52392
Independent refl.	24361	11187	15330
Observed refl. <sup>a)</sup>	13886	7520	10685
No. parameters	1569	795	913
<i>R</i> <sub>1</sub> <sup>b)</sup> ( <i>R</i> <sub>1</sub> all data)	0.046 / (0.092)	0.040 / (0.062)	0.040 / (0.065)
<i>wR</i> <sub>2</sub> <sup>c)</sup> ( <i>wR</i> <sub>2</sub> all data)	0.100 / (0.109)	0.093 / (0.098)	0.095 / (0.103)
$\Delta\rho_{\text{fin}}$ (max, min) /e·Å <sup>-3</sup>	0.61/–0.79	0.79/–0.65	0.59/–0.95

a) Observation criterion:  $I > 2\sigma(I)$ . b)  $R_1 = \sum ||F_o| - |F_c|| / \sum |F_o|$ . c)  $wR_2 = \{w \sum [w(F_o^2 - F_c^2)^2] / \sum [w(F_o^2)^2]\}^{1/2}$ .

## Acknowledgements

We are grateful to Prof. Dr. H. Krautscheid for providing facilities for X-ray crystallographic measurements. This work was supported by the Deutsche Forschungsgemeinschaft DFG-FOR 1154 “Towards molecular spintronics” and the University of Leipzig. Calculations were performed within the Cluster of Excellence “Structure Design of Novel High-Performance Materials via Atomic Design and Defect Engineering (ADDE)” that is financially supported by the European Union (European regional development fund) and by the Ministry of Science and Art of Saxony (SMWK). Computer time from the computer center at the University of Leipzig is gratefully acknowledged. We thank the ZIH Dresden for providing computational resources and support. J. Lach and E. Perlt thank the SAB for ESF grants.

## References

- U. Lehmann, J. Klingele, V. Lozan, G. Steinfeld, M. H. Klingele, S. Käss, A. Rodenstein, B. Kersting, *Inorg. Chem.* **2010**, *49*, 11018–11029.
- V. Lozan, J. Lach, B. Kersting, *Inorg. Chem.* **2012**, *51*, 5213–5223.
- J. Lach, S. V. Voitekhovich, V. Lozan, P. N. Gaponik, O. A. Ivashkevich, J. Lincke, D. Lässig, B. Kersting, *Z. Anorg. Allg. Chem.* **2010**, *636*, 1980–1986.
- V. Lozan, S. V. Voitekhovich, P. N. Gaponik, O. A. Ivashkevich, B. Kersting, *Z. Naturforsch. B* **2008**, *63*, 496–502.
- S. V. Voitekhovich, R. Syre, J. Lach, V. E. Matulis, P. N. Gaponik, O. A. Ivashkevich, B. Kersting, *Eur. J. Inorg. Chem.* **2010**, 5387–5393.
- B. Kersting, *Activating Unreactive Substrates, The Role of Secondary Interactions*, Wiley-VCH, Weinheim, Germany **2009**, ch. 1, p. 1–17.
- J. Hausmann, S. Käss, S. Klod, E. Kleinpeter, B. Kersting, *Eur. J. Inorg. Chem.* **2004**, 4402–4411.
- J. Lach, T. Hahn, B. Kersting, J. Kortus, *Eur. J. Inorg. Chem.* **2012**, 2381–2388.
- I. K. Adzamlı, K. Libson, J. D. Lydon, R. C. Elder, E. Deutsch, *Inorg. Chem.* **1979**, *18*, 303–311.
- V. E. Kaasjager, E. Bouwman, S. Gorter, J. Reedijk, C. A. Grapperhaus, J. H. Reibenspies, J. J. Smee, M. Y. Darensbourg, A. Derecskei-Kovacs, L. M. Thomson, *Inorg. Chem.* **2002**, *41*, 1837–1844.
- C. A. Grapperhaus, M. Y. Darensbourg, *Acc. Chem. Res.* **1998**, *31*, 451–459.
- R. K. Henderson, E. Bouwman, A. L. Spek, J. Reedijk, *Inorg. Chem.* **1997**, *36*, 4616–4617.
- K. Nakamoto, *Infrared and Raman Spectra of Inorganic and Coordination Compounds, Part B: Applications in Coordination, Organometallic, and Bioinorganic Chemistry*, 6th ed., Wiley, Hoboken, N. J. **2009**.
- K. Brandenburg, *Diamond*, Crystal Impact GbR, Bonn **2011**.
- C. D. Gutsche, *Calixarenes, An Introduction*, 2nd ed., RSC Publication, Cambridge **2008**.
- G. I. Koldobskii, V. A. Ostrovskii, V. S. Popavskii, *Chem. Heterocycl. Compd.* **1981**, *17*, 965–988.
- R. Goddard, O. Heinemann, C. Krüger, *Acta Crystallogr., Sect. C* **1997**, *53*, 590–592.
- Y. Ohno, Y. Akutsu, M. Arai, M. Tamura, T. Matsunaga, *Acta Crystallogr., Sect. C* **1999**, *55*, 1014–1016.
- O. Kahn, *Molecular Magnetism*, VCH-Publishers, New York, USA, **1993**.
- R. T. Azaah, L. R. Kneller, Y. Qiu, P. L. W. Tregenna-Piggott, C. M. Brown, J. R. D. Copley, R. M. J. Dimeo, *J. Res. Natl. Inst. Stand. Technol.* **2009**, *114*, 341–358.
- D. M. Duggan, E. K. Barefield, D. N. Hendrickson, *Inorg. Chem.* **1973**, *12*, 985–991.
- Y. Krupskaya, A. Alfonsov, A. Parameswaran, V. Kataev, R. Klingeler, G. Steinfeld, N. Beyer, M. Gressenbuch, B. Kersting, B. Büchner, *ChemPhysChem* **2010**, *11*, 1961–1970.
- A. P. Ginsberg, *J. Am. Chem. Soc.* **1980**, *102*, 111–117.
- L. Noodleman, *J. Chem. Phys.* **1981**, *74*, 5737–5743.
- L. Noodleman, E. R. Davidson, *Chem. Phys.* **1986**, *109*, 131–143.
- A. Bencini, D. Gatteschi, *J. Am. Chem. Soc.* **1986**, *108*, 5763–5771.
- K. Yamaguchi, Y. Takahara, T. Fueno, in: *Applied Quantum Chemistry, Proceedings of the Nobel Laureate Symposium on Applied Quantum Chemistry in Honor of G. Herzberg* [u.a.], Honolulu, HI, 16–21 Dec. **1984** (Ed.: V. H. Smith), Reidel, Dordrecht **1986**.

- [28] T. Soda, Y. Kitagawa, T. Onishi, Y. Takano, Y. Shigeta, H. Nagao, Y. Yoshioka, K. Yamaguchi, *Chem. Phys. Lett.* **2000**, *319*, 223–230.
- [29] V. Lozan, C. Loose, J. Kortus, B. Kersting, *Coord. Chem. Rev.* **2009**, *253*, 2244–2260.
- [30] P. W. Anderson, *Phys. Rev.* **1950**, *79*, 350–356.
- [31] P. W. Anderson, *Phys. Rev.* **1959**, *115*, 2–13.
- [32] J. B. Goodenough, *Phys. Rev.* **1955**, *100*, 564–573.
- [33] J. B. Goodenough, A. L. Loeb, *Phys. Rev.* **1955**, *98*, 391–408.
- [34] J. Kanamori, *J. Phys. Chem. Solids* **1959**, *10*, 87–98.
- [35] P. J. Hay, J. C. Thibeault, R. Hoffmann, *J. Am. Chem. Soc.* **1975**, *97*, 4884–4899.
- [36] *X-AREA*, Stoe & Cie, Darmstadt **2006**.
- [37] a) G. M. Sheldrick, G. M. *SHELXL-97*, Computer program for Crystal Structure Refinement, University of Göttingen, Göttingen, Germany, **1997**; b) G. M. Sheldrick, *Acta Crystallogr., Sect. A* **2008**, *64*, 112–122.
- [38] F. H. Allen, O. Kennard, D. G. Watson, L. Brammer, A. G. Orpen, R. Taylor, *J. Chem. Soc. Perkin Trans. 2* **1987**, 1–19.
- [39] A. Schäfer, H. Horn, R. Ahlrichs, *J. Chem. Phys.* **1992**, *97*, 2571–2577.
- [40] F. Weigend, R. Ahlrichs, *Phys. Chem. Chem. Phys.* **2005**, *7*, 3297–3305.
- [41] F. Neese, *WIREs Comput. Mol. Sci.* **2012**, *2*, 73–78.
- [42] P. A. M. Dirac, *Proc. Roy. Soc.* **1929**, *A123*, 714–733.
- [43] J. Slater, *Phys. Rev.* **1951**, *81*, 385–390.
- [44] A. D. Becke, *J. Chem. Phys.* **1993**, *98*, 5648–5652.
- [45] A. D. Becke, *Phys. Rev. A* **1988**, *38*, 3098–3100.
- [46] C. Lee, W. Yang, R. G. Parr, *Phys. Rev. B* **1988**, *37*, 785–789.
- [47] W. Humphrey, A. Dalke, K. Schulten, *J. Mol. Graph.* **1996**, *14*, 33–38.

Received: November 16, 2012  
Published Online: February 18, 2013